

## Coupled hydrogeophysical inversion using time-lapse magnetic resonance sounding and time-lapse gravity data for hydraulic aquifer testing: Will it work in practice?

Daan Herckenrath,<sup>1</sup> Esben Auken,<sup>2</sup> Lars Christiansen,<sup>1</sup> Ahmad A. Behroozmand,<sup>2</sup> and Peter Bauer-Gottwein<sup>1</sup>

Received 14 January 2011; revised 18 November 2011; accepted 15 December 2011; published 26 January 2012.

[1] Temporal changes in water content can be directly related to the time-lapse signals retrieved using magnetic resonance sounding (TL-MRS) and relative gravimetry (TL-RG). Previous studies suggest that TL-RG measurements can potentially provide accurate estimates of aquifer characteristics in an aquifer pumping test experiment when used in a coupled hydrogeophysical inversion approach. However, these studies considered highly idealized conditions. The aim of this paper is twofold: first, we investigate three major issues which likely limit the practical utility of TL-RG for pumping test monitoring: partially penetrating pumping wells in anisotropic aquifers, delayed drainage effects, and typical data errors for TL-RG. Second, we introduce TL-MRS in a similar coupled hydrogeophysical inversion framework and compare the performance of TL-MRS and TL-RG for pumping test monitoring. For this purpose we consider a virtual pumping test, for which we generate synthetic drawdown, TL-MRS and TL-RG observations, and subsequently determine the aquifer parameters in an inverse parameter estimation approach. The inclusion of TL-RG and TL-MRS data did slightly improve parameter estimates for the specific yield and hydraulic conductivity when considering a fully penetrating well and minimal data error. Using more conservative TL-RG and TL-MRS data error estimates according our own field experience strongly limited the informative value of the TL-RG data; TL-MRS data was less affected by this. For a partially penetrating well under anisotropic conditions, parameter uncertainty could be reduced more effectively compared to a fully penetrating well. Delayed drainage effects did not limit the ability of the TL-MRS and TL-RG data to reduce parameter uncertainty significantly. The incorporation of representative measurement error correlation in the TL-RG data did not affect its informative value. A local sensitivity analysis showed that observations were most sensitive to the pumping rate and the thickness, specific yield, and hydraulic conductivity of the aquifer. The inclusion of TL-MRS data proved to be more effective to constrain the aquifer parameters compared with TL-RG. The inclusion of both TL-RG and TL-MRS had limited added value compared to TL-MRS only. We conclude that this particular application of coupled hydrogeophysical inversion has limited potential for TL-RG, while TL-MRS appears to be a more promising method.

**Citation:** Herckenrath, D., E. Auken, L. Christiansen, A. A. Behroozmand, and P. Bauer-Gottwein (2012), Coupled hydrogeophysical inversion using time-lapse magnetic resonance sounding and time-lapse gravity data for hydraulic aquifer testing: Will it work in practice?, *Water Resour. Res.*, 48, W01539, doi:10.1029/2011WR010411.

### 1. Introduction

[2] The application of geophysical techniques in combination with hydrologic models has gained much interest in recent years to map subsurface structures and to estimate hydrologic properties [Vereecken *et al.*, 2006]. Hinnell

*et al.* [2010] and Ferré *et al.* [2009] discuss the different types of (hydro)geophysical inversion approaches that are used. Hinnell *et al.* [2010] provides an extended list of references to case study applications using different types of coupling approaches. For example, geostatistical techniques can be employed to estimate hydrologic properties using the parameter correlation structure of geophysical models [Cassiani *et al.*, 1998; Hubbard *et al.*, 1999; Yeh *et al.*, 2002; Chen *et al.*, 2004]. Hyndman and Gorelick [1996], Chen *et al.* [2006], and Linde *et al.* [2006] are examples of studies where hydrologic parameters are estimated using both hydrologic and geophysical data. In many

<sup>1</sup>Department of Environmental Engineering, Technical University of Denmark, Kgs. Lyngby, Denmark.

<sup>2</sup>Department of Geoscience, Aarhus University, Aarhus, Denmark.

other studies geo-electrical [Kemna *et al.*, 2002; Vanderborght *et al.*, 2005; Cassiani *et al.*, 2006] and electromagnetic data [Binley *et al.*, 2001; Day-Lewis *et al.*, 2003; Lambot *et al.*, 2004; Looms *et al.*, 2008; Knight, 2001; Huisman *et al.*, 2003] are used to monitor temporal changes in water content or solute concentrations.

[3] Hinnell *et al.* [2010], Ferré *et al.* [2009], Kowalsky *et al.* [2005], Pollock and Cirpka [2010], and Lambot *et al.* [2006, 2009] describe a fully coupled hydrogeophysical inversion approach, in which a hydrological model is part of the geophysical inversion process and a single objective function is minimized which comprises both a geophysical and hydrological component. In other words, both the geophysical and the hydrologic model and their associated observations are used to constrain one another.

[4] An important hydrologic state variable that can be estimated using one of the above inversion approaches is soil water content. As soil water content is difficult to measure, an increasing number of techniques have been suggested to estimate water content and changes in water storage. The strength of most geophysical methods that have been proposed, are their noninvasive character and their ability to provide data with a high-spatial resolution. Current employed techniques are predominantly geo-electric methods which estimate the electrical resistivity of the subsurface, e.g., electrical resistivity tomography (ERT), and methods which estimate the relative electrical permittivity of the subsurface based on the measured speed of propagated electromagnetic waves, e.g., ground penetrating radar (GPR). Geo-electric and wave propagation methods, however, do not measure water storage directly, as a petrophysical relationship [Archie, 1942; Topp *et al.*, 1980] is needed to convert electrical resistivity and relative permittivity to soil water content. Furthermore, GPR can only be used in high-resistivity sediments.

[5] Recently, magnetic resonance sounding (MRS) and relative gravimetry (RG) have emerged as promising methods to map hydrogeological properties. RG is a well-established method to characterize geologic structures by locating paleochannels and the delineation of buried bedrock [Carmichael and Henry, 1977; Zawila *et al.*, 1997]. Time-lapse RG (TL-RG) surveys have been performed to estimate regional water storage changes and specific yield [Montgomery, 1971; Pool and Eychaner, 1995; Jacob *et al.*, 2009; Pool, 2008], record changes in land-surface elevation [Wessells and Strange, 1985], map properties of geothermal fields [Hunt, 1970, 1977], and monitor a natural gas reservoir [van Gelderen *et al.*, 1999]. Furthermore, Poeter [1990] proposed gravity surveying during an aquifer pumping test to map heterogeneities in aquifer properties around the pumping well.

[6] Magnetic resonance is well-known for its application in hospitals, where MRI (magnetic resonance imaging) has been used for imaging and medical diagnosis [Bushong, 2003; Körver *et al.*, 2010]. Furthermore, MRS has been applied to characterize porosity and fluid properties of oil wells [Coates *et al.*, 1999; Dunn *et al.*, 2002]. For hydrogeologic characterization purposes, MRS has been applied to estimate water content, hydraulic conductivity, and transmissivity [Legchenko *et al.*, 2002; Vouillamoz *et al.*, 2002; Wyns *et al.*, 2004; Lachassagne *et al.*, 2005], providing information about aquifer boundaries, specific yield,

and the pore size characteristics of the subsurface, which can be used to estimate hydraulic conductivity [Boucher *et al.*, 2009; Chalikakis *et al.*, 2008; Ezersky *et al.*, 2010; Guerin *et al.*, 2009]. As suggested by Lubczynski and Roy [2003], time-lapse MRS (TL-MRS), can be used as a monitoring tool, which has been applied by Descloitres *et al.* [2008] to monitor groundwater level fluctuations at the discharge point of a watershed in Southern India. In this paper we will use TL-MRS by directly inverting the change in the MRS signal between two soundings at the same location for different times, rather than inverting the collected MRS data at each separate sounding time.

[7] In contrast to GPR and geo-electrical methods, data retrieved with TL-MRS and TL-RG can be directly related to temporal changes in soil water content without the use of an empirical relationship such as Archie's law [Archie, 1942] and the Topp equation [Topp *et al.*, 1980]. Both techniques could offer a cost-effective alternative for monitoring wells to augment aquifer pumping tests in unconfined aquifers [Poeter, 1990; Damiata and Lee, 2006]. A major advantage of using a noninvasive geophysical method would be the higher flexibility with which water table drawdown can be measured (indirectly) at various locations around the pumping well.

[8] Two recent papers [Damiata and Lee, 2006; Blainey *et al.*, 2007] demonstrate with synthetic data sets that water table drawdown, during aquifer testing with a fully penetrating well, could possibly be monitored with TL-RG measurements. In the work of Damiata and Lee [2006], the signal-to noise ratios are investigated for such a virtual aquifer pumping test, given an instrument accuracy of 1 microGal ( $1 \mu\text{Gal} = 1 \times 10^{-8} \text{ m s}^{-2}$ ) with portable gravimeters and 0.01–0.1  $\mu\text{Gal}$  for fixed-station (absolute) gravimeters. In the work of Blainey *et al.* [2007], a coupled hydrogeophysical inversion was subsequently performed for the same synthetic example to complement the drawdown data and obtain better estimates for the specific yield and hydraulic conductivity. For their synthetic example, a fully penetrating well was considered and the aquifer was assumed to be homogeneous and isotropic.

[9] In this study, we address three major issues that can significantly limit the practical use of TL-RG data to improve the determination of aquifer properties during pumping tests as described by Damiata and Lee [2006] and Blainey *et al.* [2007]: partially penetrating pumping wells in anisotropic aquifers, delayed drainage effects, and data error on the geophysical data. Moreover, we extend the coupled inversion approach described by Blainey *et al.* [2007] to assess the potential of TL-MRS data in this framework.

[10] Most pumping tests use a partially penetrating well in an anisotropic aquifer showing delayed drainage. One important reason for using only partially penetrating wells for thick unconfined aquifers is the cost of screening their full thickness is significant. A second reason for only screening the bottom few meters of the borehole is to protect the well from contamination. In many cases, the aquifer consists of sedimentary deposits, which have an anisotropic hydraulic conductivity tensor [Boulton, 1970] where the horizontal hydraulic conductivity is much higher compared to the vertical. When aquifer tests are conducted under the

conditions of a partially penetrating well in an anisotropic aquifer (we do not consider horizontal anisotropy [Ferre and Thomasson, 2010]), measured drawdown of the free water table can be significantly smaller compared with the drawdown of the piezometric head at the well screen. This will result in much smaller TL-MRS and TL-RG signals, and thus likely limit the applicability of both data types to estimate aquifer properties.

[11] Delayed drainage denotes noninstantaneous release of water from the unsaturated zone during the pumping test. Narasimhan and Zhu [1993] showed the importance of including effects of a time-dependent drainage from the unsaturated zone in models of flow to a well in unconfined aquifers and concluded that the rate at which water is released from the unsaturated zone has a similar timescale at which pumping tests are conducted. This process will result in residual water content above the lowered water table, which influences the magnitude of the signal changes measured by TL-RG and TL-MRS.

[12] In the previous studies of Damiata and Lee [2006] and Blainey et al. [2007], the instrument precisions were used as the standard errors on synthetic data instead of typical data error levels as seen when measuring real data. In this study, we use typical data errors associated with TL-RG and TL-MRS measurements that can be obtained during field surveys with state-of-the-art equipment. In this paper “measurement error” or “data error” refers to the standard deviation of the errors associated with the hydrogeologic and the geophysical data. Recently, Christiansen et al. [2011b] and Jacob et al. [2009] published results of TL-RG surveys indicating how accurately TL-RG data can be collected. These studies indicate measurement errors in the order of 2–4  $\mu\text{Gal}$ . A survey by Chalikhakis et al. [2008] showed MRS data can be obtained with measurement error of  $\sim 10$  nV.

[13] To understand whether TL-MRS and TL-RG data have the potential to estimate aquifer properties during unconfined pumping tests, we start with the reproduction of the modeling and inversion results shown by Blainey et al. [2007]. Subsequently, a coupled hydrogeophysical inversion is performed for 16 realizations of synthetic head, TL-RG, and TL-MRS data. Then scenarios are analyzed in which we consider each of the three, previously mentioned practical issues, i.e., partially penetrating well, delayed yield, and data error. One additional scenario is used to quantify the combined effect of these limiting factors, while a final scenario takes correlated measurement error for TL-RG data into account. The results are discussed in terms of objective function plots, parameter cross-correlation, and parameter uncertainty reduction. Finally, a sensitivity analysis is performed, to identify the impact of the pumping test design variables (and aquifer properties) on the magnitude of the geophysical signals.

## 2. Methods

### 2.1. Virtual Pumping Test

[14] Figure 1 shows a schematic overview of the pumping test configuration that was used for the analysis and Table 1 lists the design parameters for the different scenarios investigated in this paper. The scenario “fully penetrating” is the same as the scenario used by Blainey et al. [2007]

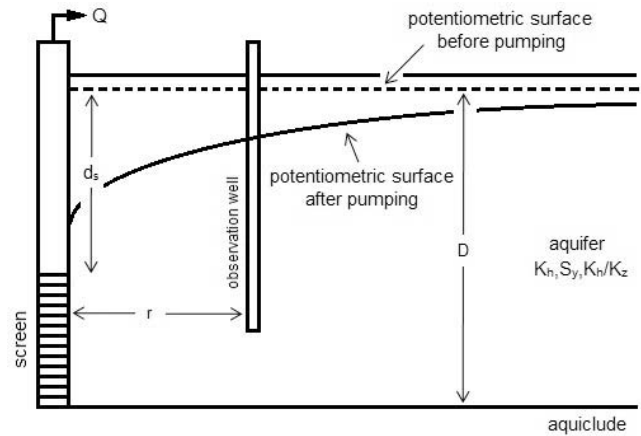


**Figure 1.** Design of a pumping test (modified from Duffield [2002]). Parameters are defined in Table 1.

and Damiata and Lee [2006]. The water table drawdown is modeled using an analytical expression derived by Moench [1997], implemented in the well-documented, widely used software WTAQ [Barlow and Moench, 1999]. Under the assumption of instantaneous release of water from storage in the unsaturated zone (instantaneous drainage), this model is equivalent to the solution by Neuman [1972, 1973].

[15] Delayed drainage effects were modeled with the approach by Boulton [1970] and Moench [1997]. In this approach, the decrease in water content in the unsaturated zone  $\Delta\theta$  [–] is modeled as an exponential function, using  $t$  [d] as the elapsed time since the time of drainage  $t_d$  [d]:

$$\Delta\theta(x, y, z, t, t_d) = S_y \left( 1 - e^{-[t-t_d \{x, y, z\}]_{\alpha_d}^{-1}} \right). \quad (1)$$

[16] In equation (1), the delay index  $1/\alpha_d$  [–] (listed in Table 1) specifies the rate of an exponential release of water from the unsaturated zone above the water table, with a maximum amount of drainable water content equal to the specific yield  $S_y$  [–].  $\Delta\theta$  equals  $S_y$  when instantaneous drainage is assumed. Values for  $1/\alpha_d$  have an approximate range of 0.5–2 d and mainly depend on the aquifer material [Moench, 1997; Rajesh et al., 2010; Boulton, 1970].

### 2.2. Time-Lapse Relative Gravity

#### 2.2.1. Modeling TL-RG Signals Caused by Water Table Drawdown

[17] During a survey with a relative gravimeter, the vertical component of the gravitational acceleration is measured, which is defined as

$$g = \int_{-\infty}^{\infty} \int_{-\infty}^{\infty} \int_{-\infty}^{\infty} \left[ G \frac{\rho(x, y, z)}{r^2} \cos \alpha \right] dx dy dz, \quad (2)$$

**Table 1.** Parameter Values and Parameters for the Different Scenarios That Were Used for the Simulations

Property	Scenario					
	Fully Penetrating	High Noise	Partially Penetrating	Delayed Yield	Partially Penetrating, Delayed Yield, and High Noise	Correlated Noise Gravity
Thickness of aquifer ( $D$ ) (m)				50		
Depth to initial water level ( $h_i$ ) (m)				25		
Hydraulic conductivity ( $K_h$ ) ( $\text{m s}^{-1}$ )				$10^{-4}$		
Anisotropy ( $K_h/K_z$ )	1	1	10	1	10	1
Specific yield ( $S_y$ )				0.25		
Radius of borehole (m)				0.1		
Well type	Fully penetrating	Fully penetrating	Partially penetrating	Fully penetrating	Partially penetrating	Fully penetrating
Screen interval, below initial water level (m)	0–50	0–50	40–50	0–50	40–50	0–50
Density of groundwater ( $\text{kg m}^{-3}$ )				1000		
Flow rate ( $Q$ ) ( $\text{m}^3 \text{s}^{-1}$ )				0.06309		
Duration of pumping ( $d$ )				7		
Locations observation wells, meters from pumping well		5, 8.3, 13.9, 23.2, 38.7, 64.6, 107.8, 179.8, 300				
Locations RG observations, meters from pumping well		5, 8.3, 13.9, 23.2, 38.7, 64.6, 107.8, 179.8, 300				
Locations MRS observations, meters from pumping well				5, 179.8		
Measurement error drawdown (cm)				5		
Measurement error TL-RG ( $\mu\text{Gal}$ )	2	4	2	2	4	4
Measurement error TL-MRS (nV)	10	20	10	10	20	—
Delay index ( $1/\alpha_d$ ) [Boulton, 1970] ( $d$ )	0	0	0	2	2	0

where  $G = 6.673 \times 10^{-11} \text{ m}^3 \text{ kg}^{-1} \text{ s}^{-2}$  is the universal gravitational constant,  $r$  [m] is the distance from the instrument to the volume element of density  $\rho$  [ $\text{kg m}^{-3}$ ], and  $\alpha$  is the angle between the orientation of  $r$  and the vertical direction. In this paper,  $\rho$  changes because of the removal of water during pumping. If storage effects, because of the compressibility of water and the aquifer matrix are neglected, the subsurface density will only change between the initial and the pumped water table. Under these assumptions the change in gravity signal  $\Delta g$  [ $\mu\text{Gal}$ ] is given by [Leirião *et al.*, 2009]

$$\Delta g(x, y) = \rho_w G \int_{-\infty}^{\infty} \int_{-\infty}^{\infty} \int_{h_i(x, y)}^{h_f(x, y)} \Delta \theta(x, y, z) \times \frac{z - z_g}{[(x - x_g)^2 + (y - y_g)^2 + (z - z_g)^2]^{3/2}} dz dx dy. \quad (3)$$

[18] This forward model is valid under the assumption of an unconfined aquifer, where the subsurface density change is equal to the density of water times the change in water content  $\Delta \theta$  of the aquifer [Leirião *et al.*, 2009]. As discussed earlier,  $\Delta \theta$  depends on the specific yield, which has a typical value between 0.01 and 0.3 for unconfined aquifers.  $h_i$  is the initial water table [m],  $h_f$  is the final water table [m], which is computed with the hydraulic model, and provides the integration bounds in the vertical direction. Subscript  $g$  denotes the  $x$ ,  $y$ , and  $z$  coordinate of the gravity instrument and  $\rho_w$  is the density of water [ $\text{kg m}^{-3}$ ]. We use an arbitrary radius of 500 m (based on an instrument footprint analysis) as the horizontal integration boundaries for equation (3). A numerical integration was performed for equation (3) using an adaptive recursive Simpson's rule

algorithm (function `dblquad` in MATLAB). The final water table  $h_f$  is location dependent and is calculated using WTAQ.

### 2.2.2. RG Instrument

[19] As a Scintrex CG-5 [Scintrex Limited, 2009] relative gravimeter is commonly used for measuring TL-RG signals, we use the specifications of this instrument to generate synthetic test data. The Scintrex CG-5 uses a fused quartz spring mechanism that reacts to changes in gravitational force. Merlet *et al.* [2008] documents an instrument accuracy of  $\sim 1 \mu\text{Gal}$  for the Scintrex CG-5 relative gravimeter.

[20] Leirião *et al.* [2009] characterize the footprint of the relative gravimeter as a function of the depth to the target. At the reference station, drawdown should be zero within the footprint of the instrument. For example, when the initial water table is at 20 m depth,  $\sim 90\%$  of the gravity signal comes from a circular area with a radius of  $\sim 200$  m.

[21] Christiansen *et al.* [2011b] provides a thorough discussion of various important corrections and precautions that need to be made when doing surveys with a relative gravimeter. For example, each time a measuring station is reoccupied, the instrument heights should be the same. When the height of a gravimeter has changed only a few millimeters between the station occupations, this will introduce an error which is comparable with the instrument resolution of  $1 \mu\text{Gal}$ . Furthermore, corrections have to be made to account for, e.g., instrument tilt, ocean loading, air pressure, tidal corrections, and ground movement. However, the magnitude of these processes still affects the accuracy with which the gravity signal is measured, as these corrections are not perfect.

[22] The measurements of relative gravimeters are also influenced by instrument drift, i.e., the zero position of the

spring does not remain constant with time. Instrument drift effects are time dependent and are caused by the instrument properties. Drift effects cannot be identified separately and are typically approximated with a linear drift coefficient for time periods of a few hours. This coefficient has a value on the order of  $20 \mu\text{Gal h}^{-1}$ . Contributions to this total drift can be subdivided into two groups: spring-aging drift and transport drift, which are discussed more thoroughly by *Christiansen et al.* [2011b]. Assuming the drift to be linear can result in correlated measurement errors induced by imperfect corrections, for example, ocean loading, as is depicted in Figure 4 in the work of *Christiansen et al.* [2011b].

[23] When measuring temporal changes in gravity signal  $\Delta g$ , typically a gravity network is repeatedly measured. During such a survey, a reference station is selected where the change in the gravity signal is assumed to be unaffected by mass changes induced by the pumping test. At the reference station the gravity value is usually set to zero. Gravity differences  $\delta g_{\text{obs}}$  are recorded with the gravimeter between the different stations of the gravity network. To calculate separate gravity values for each network station (or gravity observation point) we have to perform a network adjustment by solving equation (4), in which gravity signals  $g_{\text{est}}$  ( $\mu\text{Gal}$ ) are estimated for the different network stations together with a linear instrument drift coefficient  $c$  ( $\mu\text{Gal h}^{-1}$ ). This is done by a least-squares fit of the differences in gravimeter readings  $\delta g_{\text{obs}}$  ( $\mu\text{Gal}$ ) between the stations and the use of a design matrix ( $a_{ij}$ ) associated with the specific network configuration. The design matrix includes values of  $+1$  or  $-1$ ,  $0$ , or the time difference ( $h$ ) between two gravity measurements, where  $n$  indicates the number of gravity differences that are measured and where  $m$  marks the number of gravity stations that are occupied.

$$\begin{pmatrix} \delta g_{\text{obs},1} \\ \delta g_{\text{obs},2} \\ \vdots \\ \delta g_{\text{obs},n} \end{pmatrix} = \begin{pmatrix} a_{11} & a_{12} & \cdots & a_{1m} \\ a_{21} & \ddots & & \vdots \\ \vdots & & & \vdots \\ a_{n1} & \cdots & \cdots & a_{nm} \end{pmatrix} \begin{pmatrix} c \\ g_{\text{est},1} \\ \vdots \\ g_{\text{est},m} \end{pmatrix} + \varepsilon. \quad (4)$$

[24] After this least-squares adjustment a posteriori measurement error  $\sigma_{g_{\text{est}}}$  ( $\mu\text{Gal}$ ) (referred to as  $\sigma_{\text{GRAV}}$  [ $\mu\text{Gal}$ ]

throughout the rest of this paper) can be calculated, based on the residuals  $\varepsilon$  ( $\mu\text{Gal}$ ) and a weight matrix based on the measurement errors  $\sigma_{g_{\text{obs}}}$  ( $\mu\text{Gal}$ ) associated with the individual gravimeter readings. To obtain the temporal change in gravity signal  $\Delta g$  (equation (3)) at each gravity observation location, the same network has to be measured again at a later time in order to determine the change in  $g_{\text{est}}$ .

[25] *Christiansen et al.* [2011b] reported measurement errors  $\sigma_{\text{GRAV}}$  of  $2\text{--}3 \mu\text{Gal}$ . *Gehman et al.* [2009] reported a measurement error of  $4.76 \mu\text{Gal}$ , based on the cumulative error associated with an instrument precision of  $3 \mu\text{Gal}$  and the error resulting from uncertainties in instrument height and corrections for surface water and instrument drift. However, *Gehman et al.* [2009] did not propagate the a priori errors associated with the gravimeter readings through the network adjustment procedure. *Jacob et al.* [2009] used an approach in which the observed variance in gravimeter readings per network station were used to calculate the weight matrix associated with  $\delta g_{\text{obs}}$  and reported a  $\sigma_{\text{GRAV}}$  ranging between  $1.2\text{--}2.4 \mu\text{Gal}$ . Using the same methodology for a 2 yr survey, *Jacob et al.* [2010] published values of  $2.5\text{--}5 \mu\text{Gal}$ .

[26] To account for typical measurement errors in the analyses, we investigate uncorrelated gravity data with a measurement error  $\sigma_{\text{GRAV}}$  of  $2 \mu\text{Gal}$  and a more conservative estimate of  $4 \mu\text{Gal}$ . In addition, we perform an analysis with correlated measurement errors, in which we include one of the typical problems associated with the assumption of a linear instrument drift by adding a diurnal varying drift component that could not be captured with the linear drift coefficient [*Christiansen et al.*, 2011b].

## 2.3. Magnetic Resonance Sounding

### 2.3.1. Modeling TL-MRS Signals Caused by Water Table Drawdown

[27] With magnetic resonance sounding (MRS), the spins of the hydrogen protons of water molecules in the subsurface are excited with an external magnetic field, and the signal response resulting from precession of the protons is measured, after the external magnetic field is switched off. The quantum mechanical phenomenon of nuclear magnetic resonance can be described by the Bloch equations on the macroscopic level. The Bloch equations are the basis for modeling the MRS signal due to the water content distribution in the subsurface [e.g., *Legchenko and Valla*, 2002]

$$E(t) = - \int_{-\infty}^{\infty} \int_{-\infty}^{\infty} \int_{-\infty}^{\infty} \left[ \omega_0 M_0 \theta(x - x_{\text{MRS}}, y - y_{\text{MRS}}, z_{\text{MRS}} - z) b_{\perp}^{R_x}(x - x_{\text{MRS}}, y - y_{\text{MRS}}, z_{\text{MRS}} - z) \right. \\ \left. \times \sin\left(\frac{1}{2} \gamma b_{\perp}^{T_x} \{x - x_{\text{MRS}}, y - y_{\text{MRS}}, z_{\text{MRS}} - z\} q\right) e^{-\frac{t}{T_2^*(x - x_{\text{MRS}}, y - y_{\text{MRS}}, z_{\text{MRS}} - z)}} \right] dz dx dy, \quad (5)$$

where  $\omega_0 = \gamma B_0$ , is the angular Larmor frequency of the Earth's magnetic field  $B_0$  [T] at which the external magnetic pulse is applied.  $q = I \times \tau$  denotes the excitation pulse length, where  $I$  is the current amplitude in the transmitter loop [A] and  $\tau$  [s] is the pulse duration.  $M_0$  is the nuclear magnetization for protons in water at thermal equilibrium [A/m or J/T/m<sup>3</sup>],  $\gamma$  and  $\theta$  are the gyromagnetic ratio for the protons (0.2675 rad/s/nT) and the free water content of the subsurface [–]. Subscript MRS denotes the  $x$ ,  $y$ , and  $z$  coordinate of the MRS instrument, and  $b_{\perp}^{Tx}$  represents the magnetic field that would be created by a unit current in the transmitting antenna. For a coincident circular loop configuration (transmitter and receiver loops are the same) with a radius of  $a$  [m],  $b_{\perp}^{Rx} = b_{\perp}^{Tx} = \sqrt{(\cos[\delta]b_z + \sin[\delta]\sin[\phi]b_r)^2 + (\cos[\phi]b_r)^2}$ , where  $b_r$  and  $b_z$  are the radial and vertical components of the magnetic induction field [T/A], respectively. Angles  $\delta$  and  $\phi$  represent the inclination and the azimuth angle of the Earth's magnetic field. In the following, we assume a resistive half-space. Finite subsurface resistivity can be taken into account when interpreting MRS data [Legchenko, 2004; Braun and Yaramanci, 2008]. However, for reasons of clarity and simplicity, we use the infinite resistivity earth model. Under this assumption,  $b_r$  and  $b_z$  can be expressed in terms of elliptic integrals [Legchenko and Valla, 2002], using a composite parameter

$$m(a, r, z) = \sqrt{\frac{4ar}{(a+r)^2 + z^2}}, \quad (6)$$

where  $r$  and  $z$  are the distance and the depth with respect to the loop. The radial ( $b_r$ ) and vertical components ( $b_z$ ) of the magnetic induction field are:

$$b_r(a, r, z) = \frac{\mu}{2\pi\sqrt{(a+r)^2 + z^2}} \left[ \frac{2 \times a \times z}{(a-r)^2 + z^2} E(m[a, r, z]) - \frac{4 \times a \times z}{(a+r)^2 + z^2} F(m[a, r, z]) \right], \quad (7)$$

$$b_z(a, r, z) = \frac{\mu}{2\pi\sqrt{(a+r)^2 + z^2}} \left[ \frac{a^2 - r^2 - z^2}{(a-r)^2 + z^2} E(m[a, r, z]) + L(m[a, r, z]) \right] \quad (8)$$

with

$$L(m) = \int_0^{\pi/2} \frac{1}{\sqrt{1 - m^2(\sin[\psi])^2}} d\psi, \quad (9)$$

$$E(m) = \int_0^{\pi/2} \sqrt{1 - m^2(\sin[\psi])^2} d\psi, \quad (10)$$

$$F(m) = \frac{L(m) - E(m)}{m^2}, \quad (11)$$

[28]  $\psi$  is the horizontal angle with respect to the magnetic north and also calculated based on the Cartesian coordinates. Equation (5) was modified to simulate the temporal change in initial amplitude of the signal ( $E[t = 0]$ ), due to a change in water content  $\Delta\theta$ , which depends on the water table draw-down and specific yield of the aquifer, resulting in

$$\Delta E(q) = - \int_{-\infty}^{\infty} \int_{-\infty}^{\infty} \int_{h_i(x,y)}^{h_r(x,y)} [K(q, x - x_{\text{MRS}}, y - y_{\text{MRS}}, z_{\text{MRS}} - z) \times \Delta\theta(x, y, z)] dz dx dy \quad (12)$$

with the integration kernel:

$$\begin{aligned} K(q, x - x_{\text{MRS}}, y - y_{\text{MRS}}, z_{\text{MRS}} - z) \\ = \omega_0 M_0 b_{\perp}^{Rx} (x - x_{\text{MRS}}, y - y_{\text{MRS}}, z_{\text{MRS}} - z) \\ \times \sin\left(\frac{1}{2} \gamma b_{\perp}^{Tx} [x - x_{\text{MRS}}, y - y_{\text{MRS}}, z_{\text{MRS}} - z] q\right). \end{aligned} \quad (13)$$

[29] In this paper, we consider initial amplitude data  $E(t = 0)$  only. An alternative approach is to invert for the relaxation constant  $T_2^*$ , which can be correlated with the hydraulic conductivity of the aquifer [e.g., Mueller-Petke and Yaramanci, 2010]. To calculate the TL-MRS response based on equation (12), we use the same numerical integration method as was applied for the TL-RG forward model. During this numerical integral calculation, equation (12) is evaluated for different combinations of  $x$ ,  $y$ , and  $z$  coordinates. When these coordinates are transformed to cylindrical coordinates,  $K$  can still be solved for  $z$  are location dependent ( $x, y$ ), as in our application, the integration bounds for the depth are equal to the initial groundwater level ( $h_i$ ) and the water table during pumping ( $h_r$ ), which is calculated by the pumping test modeling software WTAQ. As we use temporal changes in MRS signal, equation (12) is applied to account for the differences in the MRS signal that are measured before and after pumping. We assume the change in the TL-MRS signal is only caused by the amount of drained water that was stored between the initial and the pumped water table.

[30] The MRS code was benchmarked against the analytical solutions presented by Legchenko and Valla [2002] for infinitely thin sheets of water with an infinite lateral extent at different depths. Figure 2 shows the values calculated with our numerical model together with the analytical solutions by Legchenko and Valla [2002], which are in good agreement. Major factors influencing the speed of our forward code were the integration bounds, the accuracy of the numerical integral evaluation, and the depth at which the sheet of water is positioned. Legchenko and Schushakov [1998] provide the definition of proper integration bounds for the MRS forward model.

### 2.3.2. MRS Instrument

[31] For generating the TL-MRS observations we consider the properties of a NUMIS<sup>plus</sup> system. The NUMIS<sup>plus</sup> device consists of an oscillating current generator, a receiver, a

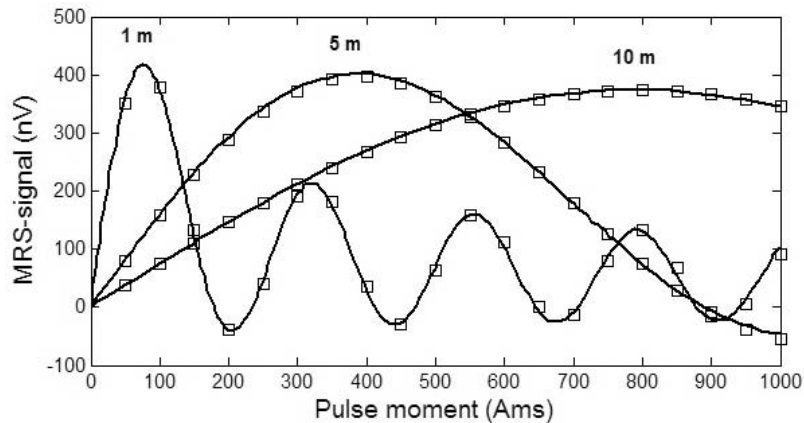


**Figure 2.** Validation numerical MRS code (squares) against infinite sheet solution (smooth lines) presented in the work of *Legchenko and Valla* [2002] for an infinite sheet of water at 1, 5, and 10 m beneath the MRS instrument for a circular loop ( $a = 50$  m) over an infinitely resistive half-space at a  $90^\circ$  magnetic inclination ( $B_0 = 60,000$  nT).

MRS signal detector, a transmitter/receiver loop, and a microprocessor. The transmitter generates the reference frequency equal to the Larmor frequency. The signal is recorded by the receiver at a frequency of 10–20 kHz and from its envelope the parameters initial amplitude  $E(t = 0)$  and relaxation time are estimated [*IRIS Instruments*, 2010]. The measured signals are affected by environmental noise sources caused by external electromagnetic interference such as electrical discharges in the atmosphere, magnetic storms, etc. Interference may also be due to the ambient noise produced by power lines and electric fences. Furthermore, the electrical resistivity of the subsurface induces attenuation of the signal as it also affects the calculation of the integration kernel ( $K$ ) of equation (12) [*Legchenko and Valla*, 2002; *IRIS Instruments*, 2010]. Note that this effect is not taken into account in our implementation as it is small for moderate and high resistivities of the ground ( $>100$  Ohm/m). Measurements are often performed in the range of 0–4 s. For a sequence of pulse lengths ( $q$ ), the noise, initial amplitude, and relaxation time are measured. The pulse lengths are often spaced densely for smaller values of  $q$  due to the high-spatial variation of the kernel function in the shallow parts. The parameters of the currently available NUMIS<sup>plus</sup> system and other surface MRS equipments do not permit measurements of very short signals (earlier times than  $\sim 20$  ms) corresponding to “bounded” water in the subsurface [*IRIS Instruments*, 2010]. As with RG, expected signal-to-noise ratios for MRS in a pumping test experiment are relatively small (compared to drawdown data). For MRS data, errors were estimated from measurements in Denmark with a NUMIS<sup>plus</sup> system presented by *Chalikakis et al.* [2008]. These results indicate that measurement errors of 10 nV can be achieved. However, in our field campaigns, we have experienced measurement errors of  $\sim 20$  nV in good noise conditions. Figure 3 shows an example plot of a noise measurement during an MRS sounding in Denmark in terms of the mean amplitude of the MRS signal. Note that the plot constitutes a single noise measurement (prestacked) and the two peaks represent the energizing pulses that are used to conduct the MRS measurements. The prestacked standard deviation of the noise is  $\sim 27$  Nv, which is a perfect condition for a MRS survey. When the

measurements are repeated a number of times (stacked), a poststacked measurement error of 20 nV can be obtained.

### 3. Coupled Hydrogeophysical Inversion

[32] A coupled hydrogeophysical inversion was carried out to estimate the specific yield  $S_y$  [–] and the hydraulic conductivity  $K_h$  [ $\text{m s}^{-1}$ ] based on drawdown data, TL-RG, and TL-MRS data. This was done in order to evaluate the value of TL-RG and TL-MRS data for six different pumping test scenarios: a fully penetrating well with low-noise geophysical data, a fully penetrating well with high-noise geophysical data, a partially penetrating well in an anisotropic aquifer, a fully penetrating well in an aquifer showing delayed drainage effects, a real-world scenario of a partially penetrating well in an anisotropic aquifer showing delayed yield in combination with high-noise geophysical data, and TL-RG data with correlated measurement errors. Table 1 summarizes the properties for the six pumping tests scenarios that were investigated. For each of these scenarios, we generated 16 different realizations of synthetic

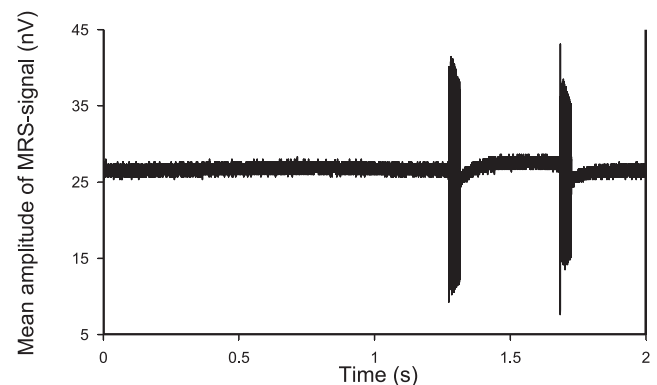


**Figure 3.** Noise measurements during an MRS sounding in Skive, Denmark. The prestacked standard deviation of the noise is  $\sim 27$  nV, indicated by the mean amplitude of the retrieved MRS signal. Two peaks of 40-ms width represent the energizing pulses injected into the loop by the instrument (double-pulse measurement).

drawdown, TL-RG, and TL-MRS measurements for subsequent parameter estimation.

### 3.1. Parameterization and Optimization Algorithm

[33] The applied coupled hydrogeophysical inversion approach proceeds as follows: first, water table drawdown is simulated with a pumping test model, with  $K_h$  and  $S_y$  as the input parameters. The simulated drawdown and  $S_y$  are then used to determine, respectively, the integration bounds and the change in water content  $\Delta\theta$  to calculate the change in the geophysical signals with the TL-MRS and TL-RG forward models.

[34] The synthetic observations are subsequently perturbed with random data error, according to the expected measurement errors for each observation type. The gradient-search algorithm PEST [Doherty, 2010] was used to iteratively update specific yield and hydraulic conductivity until the optimal fit between the synthetic observations and simulated data is achieved. Parameter starting values were varied between 0.1 and 0.4 for  $S_y$ , and  $-3.75$  and  $-4.25$  for the  $\log_{10} K_h$  (in  $\text{m s}^{-1}$ ).

### 3.2. Observations and Measurement Error

[35] To be consistent with Blainey *et al.* [2007], we consider nine observation points for drawdown and gravity measurements at 5.0, 8.3, 13.9, 23.2, 38.7, 64.6, 107.8,

179.8, and 300 m distance from the extraction well. Only two observation locations for the MRS instrument are used, situated at 5 and 179 m from the pumping well. MRS data comprises initial amplitude data measured at 8 pulse lengths between 0.5–4.0 A/s, covering a similar range as measured by Chalikakis *et al.* [2008] and example data in the NUMIS<sup>plus</sup> manual [IRIS Instruments, 2010].

#### 3.2.1. Simulated Drawdown, TL-RG, and TL-MRS Signals for a Pumping Test

[36] Figure 4a shows the water table drawdown at the nine observation points obtained after 7 d of pumping given  $K_h = 10^{-4} \text{m s}^{-1}$  and  $S_y = 0.25$  for a fully penetrating well. Figure 4b visualizes the corresponding TL-RG response for all measurement points (the same as piezometers). Figures 4c and 4d show the TL-MRS signal obtained at 5.0 and 179.8 m, respectively, from the pumping well. In the figures the standard deviation of the added measurement errors are also plotted (noise level), which were used for the generation of the synthetic observations.

[37] The plots for the partially penetrating well in Figure 4 show a significantly smaller decrease in the TL-MRS and TL-RG signals. The TL-RG signals are reduced by more than a factor of two for measurements close to the pumping well. Near the pumping well gravity changes are on the order of  $10 \mu\text{Gal}$ . The range of the received TL-MRS

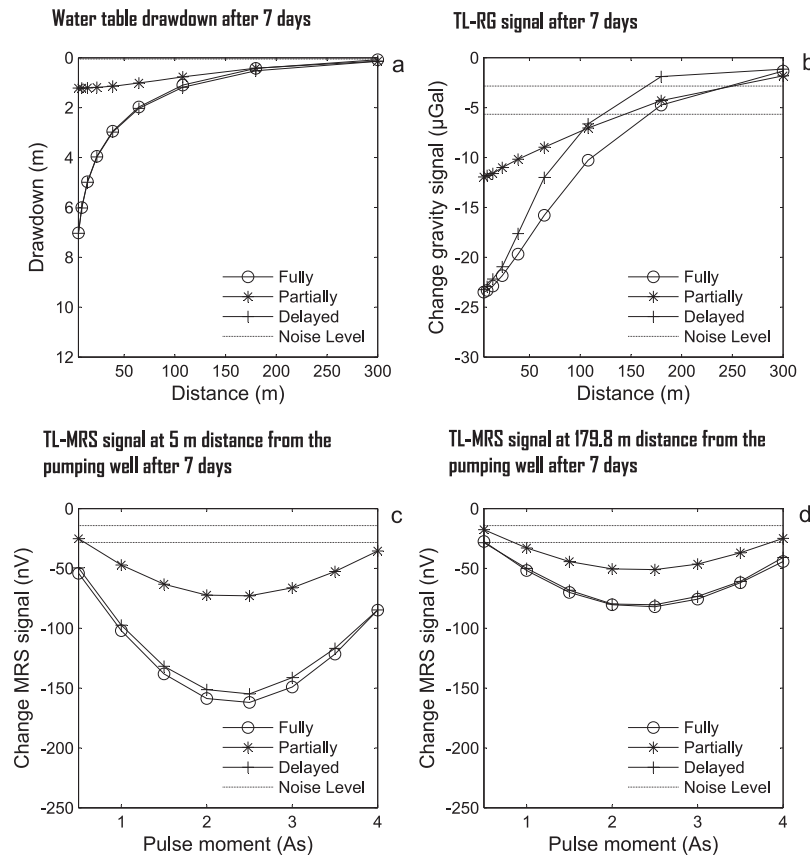


**Figure 4.** Water table (a) drawdown and (b) simulated TL-RG data after 7 d of pumping for a fully and partially penetrating well and the inclusion of delayed yield. Figures 7c and 7d show the TL-MRS signal at 5.0 and 179.8 m, respectively, from the extraction well. Note this figure shows the synthetic data without the added measurement errors. The dashed lines indicate the standard deviations of the measurement errors (noise level) that were used to generate the synthetic TL-RG and TL-MRS observations.

signal at 5 m from the pumping well is reduced from 50–150 nV to a range of 30–60 nV.

### 3.2.2. Generation of Synthetic Observations

[38] To estimate  $S_y$  and  $K_h$  we generated 16 synthetic observation sets, including drawdown, TL-RG, and TL-MRS data, to which random/uncorrelated measurement error was added. Table 1 lists the standard deviation of the applied data errors for the different observation types which were used per scenario. We assumed a measurement error of 5 cm for the drawdown data [Blainey et al., 2007], 2–4  $\mu\text{Gal}$  for the TL-RG measurements, and 10–20 nV for the TL-MRS measurements.

[39] In the scenario “correlated noise gravity” we added correlated measurement error to the TL-RG data. For this purpose, we generated a set of gravimeter readings ( $g_{\text{rel}}$ ) with a measurement error of 4  $\mu\text{Gal}$  to which we added a linear drift of 20  $\mu\text{Gal}/\text{h}$  and a sinusoidal drift component with a period of 1 d and an amplitude of 5  $\mu\text{Gal}$ . The sinusoidal drift is assumed to represent errors in the various corrections applied to the TL-RG data and is unknown for any specific field application. RG measurements in a “star”-network are assumed [Christiansen et al., 2011b], where first a reference station “REF” is measured (not impacted by the pumping test), after which each of the nine gravity observation locations  $G_i$  are occupied. The reference station is reoccupied after each station occupation (sequence REF- $G_1$ -REF- $G_2$ -...- $G_9$ -REF). Between every occupation we assume a time interval of 10 min, i.e., a total measurement period of 190 min. For each of these network stations we estimate an individual gravity signal by solving equation (4) (network adjustment), assuming a linear instrument drift. The unknown sinusoidal drift component results in correlated data errors. This procedure is executed for a time period before the pumping test starts and after 7 d of pumping. For the measurements after 7 d of pumping, we assume the sinusoidal drift component to have a 12-h phase shift compared to the prepumping survey. This numerical experiment results in one set of TL-RG observations with correlated errors. Note that error correlation in the TL-RG surveys depends on the network configuration, the magnitude of the unknown drift components, and the duration of the survey and will thus be different for every field experiment.

### 3.3. Objective Function and Parameter Uncertainty

[40] For both TL-RG and the TL-MRS we calculate the fit between the simulated and “observed” water table drawdown and geophysical data with the following objective function:

$$\begin{aligned} \phi_{\text{total}} = & (1 - w_{\text{GRAV}} - w_{\text{MRS}}) \cdot \left[ \frac{1}{N_{\text{HEADS}}} \sum_{i=1}^{N_{\text{HEADS}}} \frac{(h_{\text{meas},i} - h_{\text{sim},i})^2}{\sigma_{h_{\text{meas},i}}^2} \right]^{\frac{1}{2}} \\ & + w_{\text{GRAV}} \cdot \left[ \frac{1}{N_{\text{GRAV}}} \sum_{i=1}^{N_{\text{GRAV}}} \frac{(\text{GRAV}_{\text{meas},i} - \text{GRAV}_{\text{sim},i})^2}{\sigma_{\text{GRAV}_{\text{meas},i}}^2} \right]^{\frac{1}{2}} \\ & + w_{\text{MRS}} \cdot \left[ \frac{1}{N_{\text{MRS}}} \sum_{i=1}^{N_{\text{MRS}}} \frac{(\text{MRS}_{\text{meas},i} - \text{MRS}_{\text{sim},i})^2}{\sigma_{\text{MRS}_{\text{meas},i}}^2} \right]^{\frac{1}{2}}, \end{aligned} \quad (14)$$

where  $N_{\text{HEADS}}$  indicates the number of head data (nine in our case) and  $N_{\text{GRAV}}$  and  $N_{\text{MRS}}$  indicate the number of the different geophysical observations (nine for the TL-RG, 16 for the TL-MRS).  $h$ , GRAV, and MRS indicate the simulated and observed head, TL-RG, and TL-MRS signals.  $\sigma_h$ ,  $\sigma_{\text{GRAV}}$ , and  $\sigma_{\text{MRS}}$  represent the standard deviation of the measurement error associated with the different observations.  $w_{\text{GRAV}}$  and  $w_{\text{MRS}}$  are subjective weights defining the trade-off between the geophysical and hydrological observation misfit, where  $w_{\text{HEADS}} = 1 - w_{\text{GRAV}} - w_{\text{MRS}}$ .

[41] Determination of the optimal value for  $w_{\text{GRAV}}$  and  $w_{\text{MRS}}$  in reducing parameter uncertainty was not pursued in this research. In order to perform such a weight analysis, a Pareto method can be employed as described by Christiansen et al. [2011a] and Moore et al. [2010]. Blainey et al. [2007], using a similar model setup, report that parameter uncertainty is not very sensitive to different nonzero values of  $w_{\text{GRAV}}$ . However, they did observe a trend where larger values for  $w_{\text{GRAV}}$  result in more accurate specific yield estimates and less accurate hydraulic conductivity estimates. For this paper, we choose to use the same values for these subjective weights in order to respect their relative signal-to-noise ratios. For example, when TL-RG, TL-MRS, and drawdown data are used,  $w_{\text{GRAV}}$  and  $w_{\text{MRS}}$  are assigned a value of 1/3. For more complex hydrological models, the impact of  $w_{\text{GRAV}}$  can be of greater significance. Still, the added measurement errors could incorporate some degree of structural error, since the number of synthetically generated observations was small. This effect is reduced by performing the coupled hydrogeophysical inversion for 16 different observation realizations. Parameter uncertainty and parameter cross-correlations are subsequently estimated based on the posteriori covariance matrix for the calibrated parameter sets [Doherty, 2010].

[42] Figure 5 shows 15 objective function plots pertaining to three different situations when no measurement errors are added to the synthetically generated measurements. The first column of plots in Figure 5 shows the individual objective function components associated with the drawdown, TL-RG, and TL-MRS data and the combined objective function for a fully penetrating well when assuming unrealistically low data errors for the TL-RG and TL-MRS data (0.4  $\mu\text{Gal}$  and 2 nV, respectively) to illustrate how drawdown and geophysical data constrain one another. The plot associated with the drawdown component indicates that the hydraulic conductivity is well determined in contrast to the specific yield. Plots for the TL-RG and TL-MRS component show a nearly similar shape, illustrating that hydraulic conductivity and specific yield cannot be determined with MRS and RG data only. The combined objective function shows a clear improvement in the objective function surface highlighting a clear global minimum in comparison with the more stretched surfaces for the individual data types. The second column of plots in Figure 5 pertains to a fully penetrating well where we assume a measurement error of 5 cm for drawdown data and 2  $\mu\text{Gal}$  and 10 nV, respectively, for the gravity and MRS observations. The combined objective function surfaces do not vary significantly from the one associated with the drawdown objective function component as the signal-to-noise ratio for the geophysical data is much lower compared to the drawdown data. The third column of plots in Figure 5

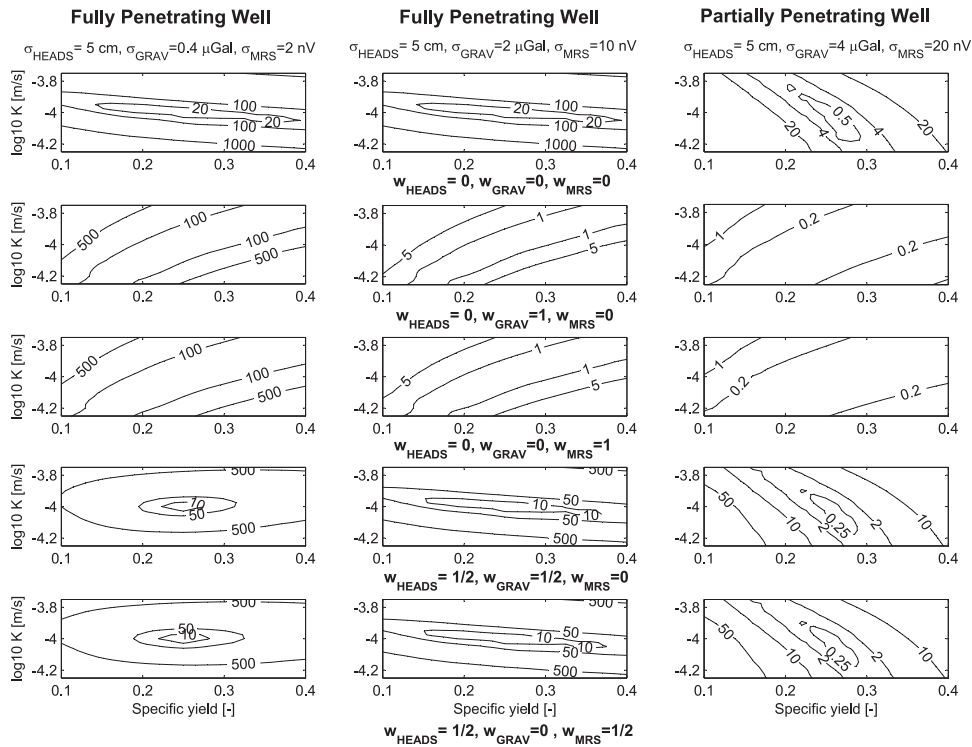


**Figure 5.** Objective function surfaces for the drawdown, gravity, and MRS objective component together with the combined objective function surfaces for a fully and partially penetrating well with a  $S_y = 0.25$  and  $K_h = 10^{-4} \text{ m s}^{-1}$ . Weights for each data type that contribute to the objective function are plotted underneath. The first column of plots pertains to TL-MRS and TL-RG data with unrealistically small measurement errors ( $0.4 \mu\text{Gal}$ ,  $2 \text{ nV}$ ). The second column represents a fully penetrating well in combination with typical signal-to-noise ratios ( $0.05 \text{ m}$ ,  $2 \mu\text{Gal}$ ,  $10 \text{ nV}$ ) for the different data types. The third column represents a partially penetrating well in combination with typical signal-to-noise ratios for the different data types, clearly showing a different orientation of the objective function surface pertaining to the drawdown and the geophysical data.

applies to a partially penetrating well in anisotropic conditions. The plots for the TL-RG and TL-MRS data show a similar pattern compared with the fully penetrating well. The drawdown objective function plot shows that the hydraulic conductivity cannot be resolved as well as for the fully penetrating well. Combining the drawdown and geophysical data in this situation could potentially be very powerful, as the objective function valleys associated with the geophysical data have a different orientation compared with the drawdown component, allowing for a well-defined global minimum. However, the information contained in the geophysical data is reduced, due to much smaller signal-to-noise ratios. This causes the combined objective functions in Figure 5 (column 3, rows 4 and 5) to have a nearly similar shape as the drawdown objective function.

## 4. Inversion Results

### 4.1. Fully Penetrating Well

[43] To assess to what extent the addition of the TL-MRS and TL-RG observations improve the estimation of the specific yield and hydraulic conductivity, cross-correlation values between the specific yield and hydraulic conductivity and their uncertainty are listed in Table 2 for each of the scenarios discussed in this paper. Note that the

values listed in Table 2 are average values pertaining to the inversion results of 16 different observation realizations that were used to calculate each scenario listed in Table 1. For a fully penetrating well, parameter cross-correlation indicates that both parameters can be identified separately, since its value is significantly smaller than 1.00. However, because of the low sensitivity of the specific yield with respect to the drawdown measurements [Blainey *et al.*, 2007], the uncertainty range for this parameter is rather large. When introducing TL-MRS or TL-RG measurements in the inverse process, which are more sensitive to the specific yield of the aquifer, parameter cross-correlation drops from  $-0.86$  to  $-0.80$  and  $-0.82$ , respectively. This also results in a decrease of the uncertainty ranges for the specific yield and hydraulic conductivity with  $\sim 30\%$ ; average parameter estimates do not change significantly for the different calibration data sets. Parameter uncertainty bounds, calculated based on the posteriori covariance matrix, show the “true” aquifer properties were captured within two standard deviations of the estimated parameter values.

[44] Table 2 shows that the uncertainty range associated with the specific yield drops from 0.022 to 0.016 when TL-RG observations are incorporated. Blainey *et al.* [2007] reported values of 0.020 and 0.012, respectively, with and without the use of TL-RG measurements. Parameter

**Table 2.** Inversion Results for the Hydraulic Conductivity and Specific Yield for Different Observation Data Sets and Each Scenario Described in Table 1

Calibration Data Set	RMSE <sup>a</sup>	Cr-Corr <sup>b</sup> $S_y$ - $K_h$	$K_h^c$ (m s <sup>-1</sup> )	Parameter Uncertainty (%) <sup>d</sup>	Uncertainty Reduction (%) <sup>e</sup>	$S_y^c$ (-)	Parameter Uncertainty (%) <sup>d</sup>	Uncertainty Reduction [%]	Scenario
Truth	-	-	1.10-4	-	-	0.25	-	-	Truth
Heads	0.82	-0.86	$9.99 \times 10^{-5} \pm 2.35 \times 10^{-6}$	2%	-	$0.251 \pm 0.022$	9%	-	Fully penetrating
Gravity	0.77	1.00	$1.07 \times 10^{-4} \pm 2.60 \times 10^2$	$\gg 100\%$	-	$0.259 \pm 2.248$	$\gg 100\%$	-	-
MRS	0.86	0.99	$1.07 \times 10^{-4} \pm 1.96 \times 10^{-4}$	$\gg 100\%$	-	$0.278 \pm 0.339$	$\gg 100\%$	-	-
Heads and gravity	0.86	-0.80	$1.00 \times 10^{-4} \pm 1.79 \times 10^{-6}$	2%	24%	$0.250 \pm 0.016$	6%	27%	-
Heads and MRS	0.92	-0.82	$9.98 \times 10^{-5} \pm 1.58 \times 10^{-6}$	2%	33%	$0.252 \pm 0.014$	6%	34%	-
Heads and gravity and MRS	0.92	-0.77	$1.00 \times 10^{-4} \pm 1.45 \times 10^{-6}$	1%	38%	$0.251 \pm 0.013$	5%	42%	-
Heads	0.82	-0.86	$9.99 \times 10^{-5} \pm 2.35 \times 10^{-6}$	2%	-	$0.251 \pm 0.022$	9%	-	-
Heads and gravity	0.93	-0.84	$9.99 \times 10^{-5} \pm 2.08 \times 10^{-6}$	2%	11%	$0.252 \pm 0.019$	8%	12%	-
Heads and MRS	0.95	-0.85	$1.00 \times 10^{-4} \pm 1.73 \times 10^{-6}$	2%	26%	$0.250 \pm 0.016$	6%	28%	-
Heads and gravity and MRS	0.92	-0.84	$1.00 \times 10^{-4} \pm 1.74 \times 10^{-6}$	2%	26%	$0.251 \pm 0.016$	6%	27%	-
Heads	0.83	-0.87	$9.99 \times 10^{-5} \pm 2.43 \times 10^{-6}$	2%	-	$0.251 \pm 0.023$	9%	-	-
Heads and gravity	0.86	-0.83	$1.00 \times 10^{-4} \pm 1.89 \times 10^{-6}$	2%	22%	$0.250 \pm 0.018$	7%	24%	-
Heads and MRS	0.93	-0.83	$9.98 \times 10^{-5} \pm 1.60 \times 10^{-6}$	2%	34%	$0.252 \pm 0.015$	6%	35%	-
Heads and gravity and MRS	0.92	-0.79	$1.00 \times 10^{-4} \pm 1.49 \times 10^{-6}$	1%	39%	$0.251 \pm 0.014$	5%	41%	-
Heads	0.76	-0.97	$1.01 \times 10^{-4} \pm 5.91 \times 10^{-5}$	58%	-	$0.250 \pm 0.057$	23%	-	-
Heads and gravity	0.83	-0.96	$1.04 \times 10^{-4} \pm 4.97 \times 10^{-5}$	33%	42%	$0.247 \pm 0.036$	14%	38%	-
Heads and MRS	0.90	-0.93	$9.74 \times 10^{-5} \pm 3.02 \times 10^{-5}$	31%	49%	$0.254 \pm 0.033$	13%	43%	-
Heads and gravity and MRS	0.83	-0.92	$9.94 \times 10^{-5} \pm 2.91 \times 10^{-5}$	29%	51%	$0.251 \pm 0.032$	13%	44%	-
Heads	0.77	-0.98	$1.02 \times 10^{-4} \pm 4.46 \times 10^{-5}$	44%	-	$0.250 \pm 0.061$	25%	-	-
Heads and gravity	0.92	-0.97	$1.00 \times 10^{-4} \pm 3.61 \times 10^{-5}$	36%	19%	$0.250 \pm 0.052$	21%	15%	-
Heads and MRS	0.92	-0.97	$1.00 \times 10^{-4} \pm 2.81 \times 10^{-5}$	27%	37%	$0.249 \pm 0.041$	16%	34%	-
Heads and gravity and MRS	0.96	-0.97	$1.00 \times 10^{-4} \pm 2.76 \times 10^{-5}$	27%	38%	$0.251 \pm 0.040$	16%	34%	-
Heads and gravity	0.84	-0.84	$1.00 \times 10^{-4} \pm 1.97 \times 10^{-6}$	2%	16%	$0.250 \pm 0.018$	7%	17%	-

Results show data misfit, parameter cross-correlation, estimated values, uncertainty ranges, and uncertainty reduction percentages.

<sup>a</sup>Root-mean-square error.

<sup>b</sup>Cross-correlation.

<sup>c</sup>Mean  $\pm 2$  standard deviations.

<sup>d</sup>Relative to the estimated parameter value.

<sup>e</sup>Percentual decrease of parameter uncertainty.

uncertainties listed in Table 2 are slightly higher due to the larger amount of measurement errors added to the drawdown (0.05 m instead of 0.045 m) and TL-RG observations (2  $\mu$ Gal instead of 1  $\mu$ Gal). Table 2 shows the same potential, if not more, for the inclusion of TL-MRS observations in reducing parameter uncertainty for this setup of aquifer testing. Parameter uncertainty for the specific yield dropped to 0.014. Therefore, a last inversion exercise was conducted in which drawdown, TL-RG, and TL-MRS observations were included. This yielded an accuracy of 0.013 in determining the value for the specific yield, which is a reduction of  $\sim 50\%$  of the original uncertainty range (when only head data composes the calibration data set). Similar values apply for the estimation of the hydraulic conductivity. As Table 2 shows, improvements are small relative to the estimated parameter values.

#### 4.2. Partially Penetrating Well in an Anisotropic Aquifer, Measurement Error, and Delayed Yield

[45] Based on our experience, 2  $\mu$ Gal and 10 nV are very optimistic estimates for the data errors encountered during field surveys with MRS and RG. For this purpose, we investigate the effect of measurement errors of 4  $\mu$ Gal and 20 nV, respectively, on the parameter estimation results in scenario “high noise.” Table 2 shows a smaller decrease in parameter correlation and parameter uncertainty reduction, especially for the TL-RG observations. Only a 12% improvement can be made in terms of parameter uncertainty reduction, which is small assuming the highly idealized conditions associated with this synthetic study. The MRS data suffers less from the increased data errors and results in an  $\sim 30\%$  uncertainty reduction.

[46] When a partially penetrating well is considered under anisotropic aquifer conditions, water table drawdown and geophysical signals are considerably smaller (Figure 4). When compared to the previous pumping scenario, the cross-correlation between the specific yield and hydraulic conductivity changes from  $-0.86$  to  $-0.97$  if aquifer properties are estimated with water table drawdown data only. When TL-RG and TL-MRS measurements are introduced, with a measurement error of 2  $\mu$ Gal and 10 nV, respectively, specific yield uncertainty ranges are reduced with  $\sim 40\%$  being more effective compared to a fully penetrating well. This can be explained by the lower information content of the drawdown data. Average parameter estimates for  $S_y$  and  $K_h$  deviate more from the true values when including the geophysical data, although the “true” aquifer properties are captured within two standard deviations of the estimated parameter values.

[47] The inclusion of delayed yield does not have a large influence on the inversion results, considering the fact we use a rather large time delay index  $1/\alpha_d$  of 2 d. This can be explained by the fact that we use drawdown, TL-MRS, and TL-RG data obtained after 7 d of pumping; this indicates the soil above the water table had enough time to release the drainable water. Inversion results are roughly the same compared to the fully penetrating well assuming instantaneous drainage.

[48] In scenario 5, we see an improvement in parameter estimates of 15% for the TL-RG data. For the TL-MRS observations, this value was  $\sim 30\%$ . However, parameter cross-correlation only decreased slightly for the inclusion

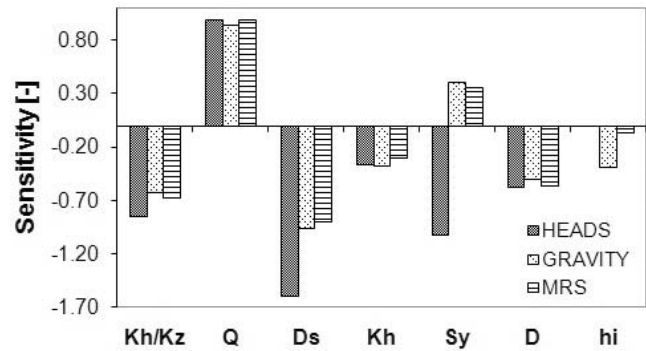


**Figure 6.** Sensitivity of drawdown, TL-MRS, and TL-RG data for seven different pumping test configurations, where in each configuration one of the original pumping test designs and configuration variables are changed. The original parameter values are those pertaining to the partially penetrating well and are listed in Table 1.

of both data types. Including both TL-RG and TL-MRS data yielded similar results compared with the inclusion of TL-MRS and drawdown data only.

[49] In the final scenario “correlated noise gravity,” we analyze the impact of correlated measurement errors for TL-RG. Comparison with the scenario “high noise,” shows there is no significant difference in the results. Parameter estimates are perfect and uncertainty ranges are comparable. While we could fit the data with a root-mean-square error (RMSE) of 0.93 in the high noise scenario, this value is now 0.84. In addition, the gravity component of the objective function remains unchanged. This could be explained by the smaller standard deviation of the added data error (for generating the correlated noise we assumed 4  $\mu$ Gal for the measurement error on the gravimeter readings, after which we performed the network adjustment). Obviously, the correlated component of the TL-RG measurement error has no significant impact, as its component could be captured assuming a linear drift in the timeframe in which we assume the TL-RG data to be collected.

#### 4.3. Sensitivity Analysis for Pumping Test Design and Aquifer Properties

[50] Section 4.2 showed that the effectiveness in reducing parameter uncertainty by including TL-MRS and/or TL-RG data strongly depends on the pumping test design and configuration. To explore the additional value of TL-MRS and TL-RG data for aquifer testing in a more general way, we conducted a local sensitivity analysis for parameters governing the pumping test design and aquifer properties with respect to the observed water table drawdown and geophysical signal changes. This sensitivity analysis was performed for the drawdown, TL-RG, and TL-MRS observations with respect to the seven different pumping test design and configuration variables that were used in the scenario “partially penetrating” ( $Q$ ,  $K_h$ ,  $h_i$ ,  $K_h/K_z$ ,  $D_s$ ,  $D$ ,  $S_y$ , which are defined in Table 1 except for  $D_s$  which represents the depth to the top of the well screen with respect to the initial water table). These sensitivities are calculated using [Hill, 1998]

$$ss_h = \frac{\Delta h/h}{\Delta p/p}, \quad (15)$$

$$ss_{\text{GRAV}} = \frac{\Delta\text{GRAV}/\text{GRAV}}{\Delta p/p}, \quad (16)$$

$$ss_{\text{MRS}} = \frac{\Delta\text{MRS}/\text{MRS}}{\Delta p/p}, \quad (17)$$

where  $ss_h$ ,  $ss_{\text{GRAV}}$ , and  $ss_{\text{MRS}}$  are the scaled sensitivities for the individual drawdown, TL-RG, and TL-MRS observations.  $p$  is the parameter value for the reference run (partially penetrating well, Table 1) and  $\Delta p$  the parameter change.  $h$ , GRAV, and MRS represent the simulated drawdown, TL-RG and TL-MRS signals for the reference run, and  $\Delta h$ ,  $\Delta\text{GRAV}$ , and  $\Delta\text{MRS}$  symbolize their change compared to the reference run. As the sign of the sensitivities for each data type was constant with respect to the different pumping test design parameters, we then calculate the sum of these scaled sensitivities ( $S_j$ ) for each separate observation group according to

$$S_j = \sum_{i=1}^{N_j} ss_i \quad \text{with } j = \text{HEADS, GRAV, MRS}, \quad (18)$$

where  $N_j$  represents the number of observations associated with every observation group (drawdown, TL-RG, and TL-MRS).

[51] Figure 6 shows the calculated sensitivities for the seven pumping test configuration parameters with respect to the total sum of water table drawdown observations (HEADS) and the geophysical signal changes (TL-RG, TL-MRS). Larger values for the hydraulic conductivity, anisotropy, aquifer depth, and depth to the pumping well screen will cause a smaller drawdown, which results in smaller TL-RG and TL-MRS signals. When the pumping rate is increased, more water mass is withdrawn resulting in larger drawdown and larger TL-RG and TL-MRS signals. Water table drawdown does not depend on the initial water table. However, both geophysical methods are sensitive to this characteristic, as stronger signal changes are observed, when mass and water content changes occur closer to the instrument. The TL-RG signal is shown to be more sensitive to the initial water table in comparison with the TL-MRS signal. Figure 6 shows an opposite sensitivity for the specific yield with respect to water table drawdown and the observed geophysical signal changes. Obviously, the higher water content that is released per volume of the subsurface outweighs the smaller drawdown that occurs. This opposite sign of the sensitivity causes the decrease in cross-correlation during the previously executed calibration exercises. According to Figure 6, the most dominant or sensitive pumping test variables are the extraction rate, anisotropy, hydraulic conductivity, and the specific yield.

## 5. Discussion and Conclusions

[52] For a pumping test, we have evaluated the inclusion of TL-RG and TL-MRS data to improve parameter estimates during unconfined aquifer testing using a coupled hydrogeophysical inversion approach. This was done by generating synthetic observations of drawdown, TL-RG, and TL-MRS data, to be used for parameter estimation. In response to the optimistic conclusions and intentions by

*Blainey et al.* [2007] and *Damiata and Lee* [2006], we first investigated the impact of three issues that will reduce the signal-to-noise ratio for TL-RG and TL-MRS measurements that could limit their additional value in the inversion process. These are a partially penetrating well in an anisotropic aquifer, typical data errors for TL-RG, and delayed yield. Furthermore, we applied the same coupled hydrogeophysical inversion framework for data acquired with TL-MRS, which was subjected to the same analysis used for TL-RG.

[53] Simulated forward responses and objective function plots showed small signal-to-noise ratios for both TL-RG and TL-MRS data for different pumping test configurations. For a fully penetrating well, considering instantaneous drainage and minimum geophysical data errors, parameter uncertainty could be reduced successfully with the incorporation of TL-RG and TL-MRS measurements, although these reductions are small relative to the parameter estimates. Incorporation of more conservative data error estimates for the TL-MRS and TL-RG observations, 20 nV and 4  $\mu\text{Gal}$ , respectively, resulted in a significant decrease of the additional value of TL-RG data. When analyzing a partially penetrating well, parameter uncertainty could be reduced more effectively with the inclusion of TL-MRS and TL-RG data when compared to a fully penetrating well. Inclusion of delayed yield did not influence the parameter estimation results significantly; however, this is also an effect of the specific setup of the synthetic study as we used measurements at a time interval where delayed yield effects are small. A scenario including a combination of the three signal-to-noise ratio reducing issues showed only a marginal improvement in parameter estimates for TL-RG. The informative value of the TL-MRS data was less affected by these. Finally, we show that typical correlated measurement errors associated with TL-RG data are not likely to influence its potential to improve the estimation of aquifer parameters. In contrast to TL-RG, we have not conducted simulations for TL-MRS data with correlated measurement errors. A local sensitivity analysis indicated that the hydraulic conductivity, thickness, and specific yield of the aquifer are the most sensitive factors, together with the extraction rate.

[54] The findings of this study suggest a limited applicability of a coupled hydrogeophysical inversion with TL-RG data for practical pumping tests, but inversion results proved to be more optimistic than we expected beforehand, especially for the partially penetrating well. The inclusion of TL-MRS data appears more promising compared to the TL-RG data, as parameter uncertainty could be reduced by  $\sim 30\%$  for most of the investigated scenarios in this work. Because of inconsistencies with *Blainey et al.* [2007] and *Damiata and Lee* [2006], we did not account for one major characteristic of practical pumping tests in our simulations, which is the fact that drawdown data often comprises a few time series rather than several drawdown measurements in space. Other important issues that were not included in this study are structural model errors, for example, due to: a heterogeneous aquifer, a slightly variable pumping rate, and the estimation of other aquifer parameters that are unknown (e.g., delay index, anisotropy, aquifer thickness).

[55] As the TL-RG and TL-MRS signals observed during a pumping test will be small in terms of signal-to-noise

ratio, a model study as presented in this paper is a necessity to assess the potential for additional TL-MRS and TL-RG observations to improve the estimates of aquifer parameters for a real-world pumping test using the coupled inversion procedure described here. This should be combined with accurate noise measurements for both techniques at the location where the pumping test is conducted. When these tests indicate whether acceptable sensitivities can be obtained for the geophysical data with respect to the aquifer parameters that are estimated, this could yield a great benefit as TL-RG and TL-MRS surveys are often much cheaper to conduct compared with the installation of a monitoring well, and no drilling is involved with these types of measurements. Another advantage of including the geophysical data, in addition to the existing drawdown observation locations, would be the reduction of the required accuracy of the drawdown measurements, which allows for a greater flexibility of picking the monitoring well locations and the use of monitoring wells that already exist at the site. As the geophysical data can yield a high-spatial resolution data set, this information would not only be suited to constrain the parameter estimation process, but can also provide much more information about the shape of the water table depression around the pumping well due to the spatial variability of the aquifer properties.

[56] **Acknowledgment.** This work was supported by the Danish Agency for Science Technology and Innovation funded project Risk-Point—assessing the risks posed by point source contamination to groundwater and surface water resources under grant 09-063216.

## References

- Archie, G. E. (1942), The electrical resistivity log as an aid in determining some reservoir characteristics, *Trans. Am. Inst. Min. Metall. Eng.*, *146*, 54–61.
- Barlow, P. M., and A. F. Moench (1999), WTAQ—a computer program for calculating drawdowns and estimating hydraulic properties for confined and water-table aquifers, *Rep. 99-4225*, 84 pp., U.S. Geol. Surv. Resour. Investigations, Northborough, Mass.
- Binley, A., P. Winship, R. Middleton, M. Pokar, and J. West (2001), High resolution characterization of vadose zone dynamics using cross-borehole radar, *Water Resour. Res.*, *37*(11), 2639–2652.
- Blainey, J. B., T. P. A. Ferré, and J. T. Cordova (2007), Assessing the likely value of gravity and drawdown measurements to constrain estimates of hydraulic conductivity and specific yield during unconfined aquifer testing, *Water Resour. Res.*, *43*(12), W12408, doi:10.1029/2006WR005678.
- Boucher, M., G. Favreau, M. Desclotres, J. M. Vouillamoz, S. Massuel, Y. Nazoumou, B. Cappelaere, and A. Legchenko (2009), Contribution of geophysical surveys to groundwater modelling of a porous aquifer in semiarid Niger: An overview, *Comptes Rendus Geoscience*, *341*(10–11), 800–809.
- Boulton, N. S. (1970), Analysis of data from pumping tests in unconfined anisotropic aquifers, *J. Hydrol.*, *10*(4), 369–378.
- Braun, M., and U. Yaramanci (2008), Inversion of resistivity in magnetic resonance sounding, *J. Appl. Geophys.*, *66*(3–4), 151–164.
- Bushong, S. C. (2003), *Magnetic Resonance Imaging: Physical and Biological Principles*, 528 pp., Mosby, St. Louis, Mo.
- Carmichael, R. S., Henry, G. Jr. (1977), Gravity exploration for groundwater and bedrock topography, *Geophysics*, *42*, 850–859.
- Cassiani, G., G. Böhm, A. Vesnaver, and R. Nicolich (1998), A geostatistical framework for incorporating seismic tomography auxiliary data into hydraulic conductivity estimation, *J. Hydrol.*, *206*, 58–74.
- Cassiani, G., V. Bruno, A. Villa, N. Fusi, and A. Binley (2006), A saline tracer test monitored via time-lapse surface electrical resistivity tomography, *J. Appl. Geophys.*, *59*, 244–256.
- Chalikakis, K., M. R. Nielsen, and A. Legchenko (2008), MRS applicability for a study of glacial sedimentary aquifers in Central Jutland, Denmark, *J. Appl. Geophys.*, *66*(3–4), 176–187.
- Chen, J. S., S. Hubbard, Y. Rubin, C. Murray, E. Roden, and E. Majer (2004), Geochemical characterization using geophysical data and Markov chain Monte Carlo methods: A case study at the South Oyster bacterial transport site in Virginia, *Water Resour. Res.*, *40*, W12412, doi:10.1029/2003WR002883.
- Chen, J., S. Hubbard, J. Peterson, K. Williams, M. Fienen, P. Jardine, and D. Watson (2006), Development of a joint hydrogeophysical inversion approach and application to a contaminated fractured aquifer, *Water Resour. Res.*, *42*, W06425, doi:10.1029/2005WR004694.
- Christiansen, L., P. J. Binning, D. Rosbjerg, O. B. Andersen, and P. Bauer-Gottwein (2011a), Using time-lapse gravity for groundwater model calibration: An application to alluvial aquifer storage, *Water Resour. Res.*, *47*, W06503, doi:10.1029/2010WR009859.
- Christiansen, L., S. Lund, O. B. Andersen, P. J. Binning, D. Rosbjerg, and P. Bauer-Gottwein (2011b), Measuring gravity change caused by water storage variations: Performance assessment under controlled conditions, *J. Hydrol.*, *402*(1–2), 60–70.
- Coates, G. R., L. Xiao, and M. G. Prammer (1999), *NMR Logging Principles and Applications*, 233 pp., Halliburton, Houston, Tx.
- Damiata, B. N., and T. C. Lee (2006), Simulated gravitational response to hydraulic testing of unconfined aquifers, *J. Hydrol.*, *318*(1–4), 348–359.
- Day-Lewis, F. D., J. W. Lane Jr., J. M. Harris, and S. M. Gorelick (2003), Time lapse imaging of saline tracer transport in fractured rock using difference attenuation radar tomography, *Water Resour. Res.*, *39*(10), 1290, doi:10.1029/2002WR001722.
- Desclotres, M., L. Ruiz, M. Sekhar, A. Legchenko, J. J. Braun, M. S. M. Kumar, and S. Subramanian (2008), Characterization of seasonal local recharge using electrical resistivity tomography and magnetic resonance sounding, *Hydrol. Processes*, *22*(3), 384–394.
- Doherty, J. (2010), PEST: Model-independent parameter estimation, in *Watermark Numer. Comput.*, Brisbane, Queensl., Australia, available at <http://www.pesthomepage.org>.
- Duffield, G. M. (2002), AQTESOLV for Windows, Version 3.5, HydroSOLVE.
- Dunn, K.-J., D. J. Bergman, and G. A. Latorraca (2002), *Nuclear Magnetic Resonance Petrophysical and Logging Applications*, vol. 32, 293 pp., Pergamon, N. Y.
- Ezersky, M., A. Legchenko, C. Camerlynck, A. Al-Zoubi, L. Eppelbaum, S. Keydar, M. Boucher, and K. Chalikakis (2010), The Dead Sea sinkhole hazard: New findings based on a multidisciplinary geophysical study, *Zeitschrift für Geomorphologie*, *54*, 69–90.
- Ferré, T. P. A., and M. J. Thomasson (2010), Understanding the impacts of anisotropy on the extent of drawdown, *Ground Water*, *48*, 478–479.
- Ferré, T., L. Bentley, A. Binley, N. Linde, A. Kemna, K. Singha, K. Holliger, J. A., Huisman, and B. Minsley (2009), Critical steps for the continuing advancement of hydrogeophysics, *Eos Trans. AGU*, *90*(23), 200–201.
- Gehman, C. L., D. L. Harry, W. E. Sanford, J. D. Stednick, and N. A. Beckman (2009), Estimating specific yield and storage change in an unconfined aquifer using temporal gravity surveys, *Water Resour. Res.*, *45*, W00D21, doi:10.1029/2007WR006096.
- Guerin, R., J. M. Baltassat, M. Boucher, K. Chalikakis, P. Y. Galibert, J. F. Girard, V. Plagnes, and R. Valois (2009), Geophysical characterisation of karstic networks: Application to the Ouyse system (Poumeysen, France), *Comptes Rendus Geoscience*, *341*(10–11), 810–817.
- Hill, M. C. (1998), Methods and guidelines for effective model calibration, *U.S. Geol. Survey Water Resources Investigations Rep. 98-4005*, 90 pp., U.S. Geol. Surv., Denver, Colo.
- Hinnell, A. C., T. P. A. Ferré, J. A. Vrugi, J. A. Huisman, S. Moysey, J. Rings, and M. B. Kowalsky (2010), Improved extraction of hydrologic information from geophysical data through coupled hydrogeophysical inversion, *Water Resour. Res.*, *46*, W00D40, doi:10.1029/2008WR007060.
- Hubbard, S. S., Y. Rubin, and E. Majer (1999), Spatial correlation structure estimation using geophysical and hydrogeological data, *Water Resour. Res.*, *35*(6), 1809–1825.
- Huisman, J. A., S. S. Hubbard, J. D. Redman, and A. P. Annan (2003), Measuring soil water content with ground penetrating radar: A review, *Vadose Zone J.*, *2*(4), 476–491.
- Hunt, T. M. (1970), Gravity changes at Wairakei geothermal field, New Zealand, *Geol. Soc. Am. Bull.*, *81*, 529–535.
- Hunt, T. M. (1977), Recharge of water in Wairakei geothermal field determined from repeat gravity measurements, *New Zealand J. Geol. Geophys.*, *20*, 303–317.
- Hyndman, D. W., and S. M. Gorelick (1996), Estimating lithologic and transport properties in three dimensions using seismic and tracer data: The Kesterson aquifer, *Water Resour. Res.*, *32*(9), 2659–2670.

- IRIS Instruments (2010), NUMIS Poly: Multi-Channel MRS System Magnetic Resonance System—User's Manual, 32 pp.
- Jacob, T., J. Chery, R. Bayer, N. Le Moigne, J.-P. Boy, P. Vernant, and F. Boudin (2009), Time-lapse surface to depth gravity measurements on a karst system reveal the dominant role of the epikarst as a water storage entity, *Geophys. J. Internatl.*, *177*(2), 347–360.
- Jacob, T., R. Bayer, J. Chery, and N. Le Moigne (2010), Time-lapse micro-gravity surveys reveal water storage heterogeneity of a karst aquifer, *J. Geophys. Res.*, *115*, B06402, doi:10.1029/2009JB006616.
- Kemna, A., J. Vanderborght, B. Kulesa, and H. Vereecken (2002), Imaging and characterization of subsurface solute transport using electrical resistivity tomography (ERT) and equivalent transport models, *J. Hydrol.*, *267*, 125–146.
- Knight, R. (2001), Ground penetrating radar for environmental applications, *Annu. Rev. Earth Planet. Sci.*, *29*, 229–255.
- Körver, R. J. P., P. H. M. H. Theunissen, W. T. van de Kreeke, M. J. A. van der Linde, and I. C. Heyligers (2010), Juxta-articular myxoma of the knee in a 5-year-old boy: A case report and review of the literature (2009: 12b), *European Radiol.*, *20*, 764–768.
- Kowalsky, M. B., S. Finsterle, J. Peterson, S. Hubbard, Y. Rubin, E. Majer, A. Ward, and G. Gee (2005), Estimation of field-scale soil hydraulic and dielectric parameters through joint inversion of GPR and hydrological data, *Water Resour. Res.*, *41*, W11425, doi:10.1029/2005WR004237.
- Lachassagne, P., J. M. Baltassat, A. Legchenko, and H. Machard de Gramont (2005), The links between MRS parameters and the hydrogeological parameters, *Near Surf. Geophys.*, *3*(4), 259–265.
- Lambot, S., M. Antoine, I. van den Bosch, E. C. Slob, and M. Vanclooster (2004), Electromagnetic inversion of GPR signals and subsequent hydrodynamic inversion, *Vadose Zone J.*, *3*, 1072–1081.
- Lambot, S., E. C. Slob, M. Vanclooster, and H. Vereecken (2006), Closed loop GPR data inversion for soil hydraulic and electric property determination, *Geophys. Res. Lett.*, *33*, L21405, doi:10.1029/2006GL027906.
- Lambot, S., E. Slob, J. Rhebergen, O. Lopera, K. Z. Jadoon, and H. Vereecken (2009), Remote estimation of the hydraulic properties of a sand using full-waveform integrated hydrogeophysical inversion of time-lapse, off-ground GPR data, *Vadose Zone J.*, *8*, 743–754.
- Legchenko, A. (2004), Magnetic resonance sounding: Enhanced modeling of a phase shift, *Appl. Magnetic Resonance*, *25*(3–4):621–636.
- Legchenko, A., and O. Shushakov (1998), Inversion of surface NMR data, *Geophysics*, *63*(1), 75–84.
- Legchenko, A., and P. Valla (2002), A review of the basic principles for proton magnetic resonance sounding measurements, *J. Appl. Geophys.*, *50*(1–2), 3–19.
- Legchenko, A., J. M. Baltassat, A. Beauce, and J. Bernard (2002), Nuclear magnetic resonance as a geophysical tool for hydrogeologists, *J. Appl. Geophys.*, *50*(1–2), 21–46.
- Leirião, S., X. He, L. Christiansen, O. B. Andersen, and P. Bauer-Gottwein (2009), Calculation of the temporal gravity variation from spatially variable water storage change in soils and aquifers, *J. Hydrol.*, *365*(3–4), 302–309.
- Linde, N., S. Finsterle, and S. Hubbard (2006), Inversion of tracer test data using tomographic constraints, *Water Resour. Res.*, *42*, W04410, doi:10.1029/2004WR003806.
- Looms, M. C., K. H. Jensen, A. Binley, and L. Nielsen (2008), Monitoring unsaturated flow and transport using cross-borehole geophysical methods, *Vadose Zone J.*, *7*, 227–237.
- Lubczynski, M., and J. Roy (2003), Hydrogeological interpretation and potential of the new magnetic resonance sounding (MRS) method, *J. Hydrol.*, *283*(1–4), 19–40.
- Merlet, S., A. Kopaeve, M. Diamant, G. Geneves, A. Landragin, and F. P. Dos Santos (2008), Micro-gravity investigations for the LNE watt balance project, *Metrologia* *45*(3), 265–274.
- Moench, A. F. (1997), Flow to a well of finite diameter in a homogeneous, anisotropic water table aquifer, *Water Resour. Res.*, *33*, 1397–1407, 593–596.
- Montgomery, E. L. (1971), Determination of specific yield using gravity measurements, *Eos Trans. AGU*, *52*, 205.
- Moore, C., T. Wohling, and J. Doherty (2010), Efficient regularization and uncertainty analysis using a global optimization methodology, *Water Resour. Res.*, *46*, W04410, doi:10.1029/2004WR003806.
- Mueller-Petke, M., and U. Yaramanci (2010), QT inversion: Comprehensive use of the complete surface NMR data set, *Geophysics*, *75*, WA199–WA209.
- Narasimhan, T. N., and M. Zhu (1993), Transient flow of water to a well in an unconfined aquifer: Applicability of some conceptual models, *Water Resour. Res.*, *29*(1), 179–191.
- Neuman, S. P. (1972), Theory of flow in unconfined aquifers considering delayed response of the water table, *Water Resour. Res.*, *8*, 1031–1045.
- Neuman, S. P. (1973), Supplementary comments on “Theory of flow in unconfined aquifers considering delayed response of the water table,” *Water Resour. Res.*, *9*, 1102–1103.
- Poeter, E. P. (1990), A new tool: Delineation of textural heterogeneities in unconfined aquifers, using microgravity surveys during pumping, *Bull. Assoc. Eng. Geol.*, *27*(3), 315–325.
- Pollock, D., and O. A. Cirpka (2010), Fully coupled hydrogeophysical inversion of synthetic salt tracer experiments, *Water Resour. Res.*, *46*, W07501, doi:10.1029/2009WR008575.
- Pool, D. (2008), The utility of gravity and water-level monitoring at alluvial aquifer wells in southern Arizona, *Geophysics*, *73*(6), WA49–WA59.
- Pool, D. R., and J. H. Eychaner (1995), Measurements of aquifer-storage change and specific yield using gravity surveys, *Ground Water*, *33*, 425–432.
- Rajesh, M., D. Kashyap, and K. S. H. Prasad (2010), Estimation of unconfined aquifer parameters by genetic algorithms, *Hydrol. Sci. J.*, *55*(3), 403–413.
- Scintrex Limited (2009), *CG-5 Scintrex Autograv System Operation ManualRrev.*, *4*, available at <http://www.scintrexlimited.com/gravity.html>.
- Topp, G. C., J. L. Davis, and A. P. Annan (1980), Electromagnetic determination of soil water content: Measurements in coaxial transmission lines, *Water Resour. Res.*, *16*(3), 574–582.
- Vanderborght, J., A. Kemna, H. Hardelauf, and H. Vereecken (2005), Potential of electrical resistivity tomography to infer aquifer transport characteristics from tracer studies: A synthetic case study, *Water Resour. Res.*, *41*, W06013, doi:10.1029/2004WR003774.
- van Gelderen, M., R. Haagmans, and M. Bilker (1999), Gravity changes and natural gas extraction in Groningen, *Geophys. Prospect.*, *47*, 979–993.
- Vereecken, H., A. Binley, G. Cassiani, A. Revil, and K. Titov (Ed.) (2006), *Applied Hydrogeophysics*, 383 pp., Springer, Dordrecht, Netherlands.
- Vouillamoz, J. M., M. Desclotres, J. Bernard, P. Fourcassié, and L. Romagny (2002), Application of integrated magnetic resonance sounding and resistivity methods for borehole implementation, a case study in Cambodia, *J. Appl. Geophys.*, *50*, 67–81.
- Wessells, C. W., and W. E. Strange (1985), Results of repeat gravity measurements in areas of ground water withdrawal, *Eos Trans. AGU*, *66*, 364.
- Wyns, R., J. M. Baltassat, P. Lachassagne, A. Legchenko, and J. Vairon (2004), Application of proton magnetic resonance soundings to groundwater reserve mapping in weathered basement rocks (Brittany, France), *Bulletin de la Société géologique de France*, *175*(1), 21–34.
- Yeh, T. C. J., S. Liu, R. J. Glass, K. Baker, J. R. Brainard, D. Alumbaugh, and D. LaBrecque (2002), A geostatistically based inverse model for electrical resistivity surveys and its applications to vadose zone hydrology, *Water Resour. Res.*, *38*(12), 1278, doi:10.1029/2001WR001204.
- Zawila, J. S., B. N. Damiata, S. C. Biehler, and T. C. Lee (1997), Gravity mapping of subsurface structures in batholithic terrain, paper presented at Symposium on the Application of Geophysics to Engineering and Environmental Problems, Reno, Nevada, 801–810.

E. Atuken and A. A. Behroozmand, Department of Geoscience, Aarhus University, Høegh-Guldbergs Gade, building 1120, 8000 Aarhus, Denmark.

P. Bauer-Gottwein, L. Christiansen, and D. Herckenrath, Department of Environmental Engineering, Technical University of Denmark, Miljøvej, building 113, 2800 Kgs. Lyngby, Denmark. (daah@env.dtu.dk)